

25 **Abstract**

26 **Background:** Chronic Obstructive Pulmonary Disease (COPD) and Idiopathic
27 Pulmonary Fibrosis (IPF) are chronic, progressive lung ailments which are
28 characterized by distinct pathologies. Early detection biomarkers and disease
29 mechanisms for these debilitating diseases are lacking. Exosomes are small
30 extracellular vesicles attributed to carry proteins, mRNA, miRNA and sncRNA to
31 facilitate cell-to-cell communication under normal and diseased conditions. Exosomal
32 miRNAs have been studied in relation to many diseases. However, there is little to no
33 knowledge regarding the miRNA population of BALF or the lung tissue derived
34 exosomes in COPD and IPF. Here, we determined and compared the miRNA profiles of
35 BALF and lung tissue-derived exosomes from healthy non-smokers, healthy smokers,
36 and patients with COPD and IPF in independent cohorts. **Results:** Exosome
37 characterization using NanoSight particle tracking and TEM demonstrated that the
38 BALF-derived exosomes were approximately 89.85 nm in size and $\sim 2.95 \times 10^{10}$
39 particles/mL. Lung-derived exosomes were ~ 146.04 nm in size and $\sim 2.38 \times 10^{11}$
40 particles/mL. NGS results identified three differentially expressed miRNAs in the BALF,
41 while one in the lung-derived exosomes from COPD patients as compared to healthy
42 non-smokers. Of these, three- and five-fold downregulation of miR-122-5p amongst the
43 lung tissue-derived exosomes from COPD patients as compared to healthy non-
44 smokers and smokers, respectively. Interestingly, there were key 55 differentially
45 expressed miRNAs in the lung tissue-derived exosomes of IPF patients compared to
46 non-smoking controls. **Conclusions:** Overall, we identified specific miRNAs to develop
47 as biomarkers or targets for pathogenesis of these chronic lung diseases.

48 **Keywords:** Exosomes, miRNA, COPD, Biomarker, BALF and Lung tissue.

49 **Introduction**

50 Tobacco smoking remains the most prevalent preventable cause of morbidity and
51 mortality, worldwide. Comprising of more than 5000 compounds (1), cigarette smoke is
52 the leading risk-factor for developing chronic obstructive pulmonary disease (COPD)
53 and idiopathic pulmonary fibrosis (IPF) in humans. Despite their distinct clinical features,
54 both COPD and IPF can be defined as chronic, progressive airway diseases associated
55 with increased risk of cancer development (2, 3). The current therapies for these
56 conditions are mainly palliative; and the chief reason of this is due to limited
57 understanding of the pathophysiology of these respective ailments (4, 5).

58 Evidence from literature suggest the role of extracellular vesicles/exosomes in the
59 disease severity and outcome in COPD and IPF (6-10). Exosomes function to maintain
60 homeostasis and intracellular stability. However, they also become pathosomes due to
61 harmful stimulus (e.g. tobacco smoke) and can participate in the progression of
62 diseases. In this respect, exosomes are known to cause pathological changes including
63 oxidative stress, chronic inflammation, apoptosis, aging, epigenetic alterations and
64 multi-organ dysfunction in COPD (11-14). Interestingly, exosomes are produced and
65 released in the sputum, serum and BALF of COPD patients in large quantities which
66 makes them a useful target to develop non-invasive diagnostics in COPD. Previous
67 studies have mostly compared the serum-derived exosome populations from COPD
68 patients and healthy individuals (15-20). Similarly, exosomes isolated from the biological
69 fluids cause pro-inflammatory responses in lung cells (11, 21, 22). However, there is

70 little to no knowledge about the BALF or the lung tissue-derived exosome populations in
71 COPD or IPF.

72 Based on this, we compared the miRNA population in the BALF and lung tissue-derived
73 exosomes from healthy non-smokers, healthy smokers, and patients with COPD and
74 IPF in several independent cohorts. Numerous studies have shown that circulating
75 miRNAs are involved in the progression, development and severity of various diseases
76 including COPD and IPF (6, 9, 11, 23-26). These are also considered to be known
77 targets for biomarker development (27, 28). Hence, we compared the exosome-derived
78 miRNA profiles amongst COPD and IPF patients with healthy individuals to identify
79 miRNA signatures that might be unique to each of these distinct pathological conditions
80 and help determine the progress of the pulmonary damage at an early stage.

81

82 **Materials and Methods**

83 **Ethics/Approval**

84 The human patients and the patients' data included in the study were procured from
85 several agencies (described below) as human subjects were not directly involved in this
86 work. The procurement of human lung tissues and BALF samples as deidentified
87 samples was approved by the Materials Transfer Agreement and Procurement
88 (Institutional Review Board, IRB), and Laboratory protocols by the Institutional Biosafety
89 Committee (IBC) at the University of Rochester Medical Center, Rochester, NY. The
90 project codes and dates of approval were as follow: Project Code: DRAI1 001 Protocol:
91 004, Date of approval and IRB/IBC approvals 2/11/2017 and 9/29/2017.

92 All the procedures/ protocols were carried per the guidelines and regulations specified
93 by the University of Rochester, Rochester, NY. Other approvals include: (a) IRB study
94 number 20080326 at the University of Miami, and (b) registered clinical trial
95 (NCT04016181) and ethically approved by the University of Edinburgh (07/S1102/20)
96 and NHS Lothian 2007/R/RES/02 by 14/06/2007. Additional samples were obtained
97 from baseline measurements of Feasibility of Retinoids for the Treatment of
98 Emphysema (FORTE) trial participants as described previously (29, 30).

99

100 **Study population and Sample Collection**

101 We employed bronchoalveolar lavage fluid (BALF) and lung tissues collected from
102 healthy (Non-smokers and Smokers) and diseased (COPD and IPF) human subjects as
103 samples for this study from 7 independent cohorts (**Table 1**). A total of 40 BALF
104 samples and 32 lung tissue samples were chosen for this study from multiple sources.
105 The majority of the BALF samples used in this study were procured from a commercial
106 provider- BioIVT (Westbury, NY, USA). Rest of the BALF samples were provided by
107 our collaborators- Dr. Michael Campos from Division of Pulmonary, Allergy, Critical
108 Care at University of Miami, Dr. Hitendra Chand from Department of Immunology at
109 Florida International University, Dr. Haseeb Siddiqi from Department of Cell Biology at
110 SUNY Downstate Health Sciences University and Dr. Nikhil Hirani from Center of
111 Inflammation research at Edinburgh University, UK. The samples procured from our
112 collaborators were validated for their disease categories based on their spirometry and
113 clinical status.

114 Likewise, the lung samples were procured from three sources; (a) commercially
115 available resource for procurement of human tissue and organ- NDRI (National Disease
116 Research Interchange), (b) NHLBI-funded bio-specimen repository- LTRC (Lung Tissue
117 Research Consortium), and (c) Department of Medicine and Pathology at the University
118 of Helsinki Hospital, Finland as reported previously (31, 32).

119 All the subjects included in the study were above 21 years of age. Care was taken to
120 include equal numbers of males and females in each subject group. A detailed
121 characteristic of the BALF and Lung tissue samples used for this study is provided in
122 **Table 1.**

123 **BALF exosome isolation**

124 We employed commercially available Plasma/Serum Exosome Purification and RNA
125 Isolation Midi Kit from Norgen Biotek (Cat# 58500; Ontario, Canada) to isolate
126 exosomes from human BALF samples. BALF exosomes were isolated as per
127 manufacturer's protocol. In brief, 1 mL BALF sample was mixed with Nuclease-free
128 water, ExoC Buffer and Slurry E; and incubated for 5 minutes at room temperature.
129 Next, the solution was centrifuged at 2000 rpm for 5 min at room temperature and the
130 supernatant was discarded. The slurry pellet was then resuspended in ExoR buffer and
131 incubated for 10 min at room temperature. Thereafter the suspension was centrifuged at
132 8000 rpm for 2 min duration at room temperature and transferred to Mini Filter Spin
133 column to elute the exosomal fraction. The eluted exosomes were then stored at -80°C
134 until further use.

135 **Lung Tissue Exosome Isolation**

136 The tissue exosomes were isolated using the protocol described by Dooner et al (2018)
137 (33) with some modifications. In brief, 30-40 mg of lung tissue was chopped and lysed
138 using 1X Liberase solution containing 0.01% DNase. The tube containing tissue lysate
139 was left on an orbital shaker at 37⁰C for 1-hour duration to allow complete digestion of
140 lung tissues. After 1-hour incubation, the tissue lysate was collected. The eluate was
141 then centrifuged at 300 g for 10 min at 4⁰C to remove cell debris. Next, the supernatant
142 was transferred to fresh tube and centrifuged at 2000 g for 10 min at 4⁰C. Again, the
143 supernatant was transferred to a fresh tube and centrifuged at 10,000 g for 30 min at
144 4⁰C to remove larger vesicles. After this, the supernatant was transferred to
145 ultracentrifuge tubes and the exosomes were pelleted at 110,000g for 70 min at 4⁰C
146 using Optima Max-XP ultracentrifuge (Beckman Coulter, Brea, CA). At this stage, the
147 supernatant was discarded and the pellet was resuspended in 1X PBS prior to filtering
148 through 0.22 μ M filter. The filtrate was once again spun at 110,000g for 70 min at 4⁰C.
149 Finally, the supernatant was discarded and the pellet was re-suspended in 1mL 1X
150 PBS. This contained freshly isolated tissue exosomes that were stored at -80⁰C for
151 future analysis.

152 **Exosome Characterization**

153 We employed Hitachi 7650 Analytical transmission electron microscopy (TEM) to
154 visualize the isolated exosomes and nanoparticle tracking analysis (NanoSight NS300)
155 to analyze the particle size and concentration as described earlier (12, 34).

156 We also used immunoblotting to identify exosomal markers from the isolated fraction to
157 characterize the BALF and lung tissue derived exosomes. In brief, 20 ug of exosomal

158 lysate was resolved on a 10% sodium dodecyl sulfate (SDS)-polyacrylamide gel and
159 electroblotted onto nitrocellulose membranes. Membrane was blocked using 5%
160 blocking buffer for 1 hr and thereafter probed overnight with antibodies for exosomal
161 surface markers. The antibodies include-CD9 (Cat# ab92726), CD63 (Cat# ab134045)
162 (Abcam, Cambridge, UK) and CD81 (Cat# EXOAB-CD81A-1) (SBI Biosciences, Palo
163 Alto, CA). The following days, the blots were washed and probed with appropriate
164 secondary antibodies. Chemiluminescence was detected on the Bio-Rad ChemiDoc
165 MP, Imaging system using the SuperSignal West Femto Maximum Sensitivity Substrate
166 (Cat# 34096, Thermo Scientific, Waltham, MA).

167 **Exosomal RNA extraction**

168 Total RNA from BALF exosomes was isolated using Exosomal RNA isolation kit
169 (Norgen Bioteck Corporation, Cat# 58000) as per the manufacturer's protocol. The
170 detailed procedure has been published earlier (34).

171 Alternately, we used miRNeasy Mini Kit (Cat# 217004, Qiagen, Hilden, Germany) to
172 isolate RNA from lung exosomes as per manufacturer's protocol. Briefly, 700 µl of
173 QIAzol lysis buffer was mixed with 250 µl of exosomal fraction and the mix was
174 homogenized using QIAshredder. The homogenate was then mixed with 140µl of
175 chloroform to allow phase separation and the aqueous phase was transferred to a fresh
176 tube. Thereafter, the RNA was precipitated using 100% ethanol and washed using RWT
177 and RPE buffers provided with the kit. Finally, the RNA was eluted using RNase-free
178 water and stored at -80°C until further use. The RNA quality and quantity were checked
179 using Agilent 2100 Bioanalyzer.

180 **Library preparation**

181 The isolated RNA samples were shipped to Norgen Biotek, Canada for library
182 preparation, sequencing and data analyses. The library preparation was performed
183 using the standard library preparation workflow of Norgen including 3' and 5' adapter
184 ligation, followed by reverse transcription, indexing PCR and size selection using a 6%
185 Novex TBE Gel. In brief, Norgen Biotek Small RNA Library Prep Kit (Cat# 63600) was
186 employed for library preparation making sure to use the same lot between each batch of
187 samples.

188 Samples were quantified using both PicoGreen and Bioanalyzer. 6uL of high-quality
189 total RNA was mixed with 3' adaptor and T4 RNA ligase 2 to set up a reaction for 3'
190 Adaptor ligation per manufacturer's protocol. This was followed by the removal of
191 excess 3' Adaptor and then 10-12 µl of final eluate was mixed with 5'Adaptor to set up a
192 reaction for 5' Adaptor Ligation. Next, the reaction for cDNA synthesis was set using the
193 obtained ligated product as input, per manufacturer's directions and incubated at 50⁰C
194 for 1 hour in a thermocycler. This was followed by PCR amplification and indexing as
195 advised and cleanup of final indexed PCR product using NGS Reaction Cleanup Kit.
196 After cleaning, the samples were run on a 6% Novex TBE Gel for 50 minutes at 140V.
197 The adaptor dimer not containing any library was excised, and the sample was eluted
198 from the gel and checked for quality as per the manual's instruction. At this stage, the
199 library quality check was performed to estimate library size and concentration using
200 Bioanalyzer. Samples were then pooled in equimolar ratios and further size selected
201 using a 3% Agarose Gel cassette on the Pippin prep (Part # SAG-CDP3010). The pool

202 was quantified by Bioanalyzer before starting the Next Generation Sequencing (NGS)
203 run.

204 **Next Generation Sequencing (NGS) and Data Analysis**

205 We employed NextSeq 500/550 High Output Kit v2 for 75 cycles (Cat# 20024906,
206 Illumina, San Diego, CA) to perform NGS on our pooled library. Per the manufacturer's
207 directions the pooled library was denatured and diluted to the required concentration of
208 20pM for optimal cluster generation. Library was then applied onto the suitable flow-cell
209 and sequenced using Illumina NextSeq 500 sequencing platform.

210 The raw sequence reads were analyzed by the team of bioinformaticians at Norgen
211 using their advanced analysis pipeline for the processing of raw counts and alignment to
212 endogenous genome and annotated transcriptome.

213 **Gene Ontology and KEGG analyses**

214 The gene ontology or GO (35) enrichment analysis was performed, through the
215 examination of significant GO terms associated with the differentially expressed
216 miRNAs for each comparison group. The analysis was performed by iteratively testing
217 the enrichment of each annotated GO term correlated with the set of pre-selected
218 differentially expressed genes (in our case, miRNAs) in a linear fashion. Individual
219 enriched annotated GO terms were analyzed using a Fisher's exact test for both up-
220 regulated and down-regulated genes in which GO terms with an FDR adjusted p-value
221 threshold of 0.05 were reported as significantly relevant. The FDR is the false discovery
222 rate generated using the Benjamini-Hochberg method, which adjusts the p-value based

223 on the FDR. The analysis was performed separately on all three GO domains, i.e,
224 biological process, molecular function and cellular component.

225 The KEGG (36) enrichment analysis was also performed to identify the differentially
226 expressed genes within an associated pathway for various biological processes. The
227 analysis was performed by testing the enrichment of each biological pathway with the
228 associated gene (or miRNA) found within the set of pre-selected differentially expressed
229 genes. Individually enriched pathways were then contrasted and compared between the
230 two test groups using a Fisher's exact test for both up-regulated and down-regulated
231 genes within the pre-selected set of differentially expressed genes. Biological pathways
232 with an adjusted p-value below 0.05 were reported.

233 **Statistical analysis**

234 The miRNA data from various batches were normalized using trimmed mean of M-
235 values (TMM) normalization method (37). The TMM normalized read counts were used
236 for differential expression analysis. The Principal Component analysis (PCA) was
237 plotted using the *ggfortify* function in R-software (version: 3.5.1) to produce a sample
238 clustering plot based on miRNAs with the highest variation across all samples. The
239 coefficient of variation (% CV) was calculated based on the \log_2 of TMM normalized
240 data and then the 50 miRNAs with the highest %CV were selected and used to
241 generate the PCA plot. The highest two components of variation were plotted on the x-
242 axis (the first principal component, PCA1) and the y-axis (the second principal
243 component, PCA2). Confidence ellipses and average center points were calculated and
244 added for each sample group to further organize the biological groupings.

245 EdgeR statistical software package was used for DE analysis as described previously
246 (38, 39). The Benjamini-Hochberg procedure was then used for adjusting the false
247 discovery rate (FDR) (40). This allowed identifying the significant DE when comparing
248 two groups. The DE was considered significant if log fold change of ≥ 1 or ≤ -1 at p-
249 value and FDR of ≤ 0.05 was reported for the miRNA target. We used the *ggplot2*
250 function in R software (version: 3.5.1) to plot volcano plots for illustrating a large number
251 of miRNAs and displaying the particular miRNA targets with statistically significant
252 differential expression.

253 Heat maps were generated using the *ComplexHeatmap* function in R-software (version:
254 3.5.1). The coefficient of variation (% CV) was calculated based on \log_2 of TMM
255 normalized data and then the 50 miRNAs with the highest %CV were selected and used
256 to generate the heat map.

257 Kruskal-Wallis test was used to calculate significance for sample distribution.

258 **Results**

259 **Characterization of BALF and lung-tissue derived exosomes**

260 Exosomes are known to be involved with intercellular communication thus affecting the
261 physiological processes in various tissues. Here, we analyzed the miRNA population
262 from the BALF and lung tissue exosomes isolated from the non-smokers, smokers, and
263 the patients with COPD or IPF. We first isolated the BALF and lung tissue-derived
264 exosomes using the methods described earlier. We employed immunoblotting,
265 nanoparticle tracking analysis (NTA: NanoSight 300), and transmission electron
266 microscopy (TEM) to characterize the isolated exosomes. We first used NTA to

267 determine the particle concentration, size, or distribution of exosomes in isolated
268 samples from BALF and lung tissues. The lung-derived exosomes (avg. conc. = $2.38 \pm$
269 2.2×10^{11} particles/mL) had larger size (mean = 146.04 nm). On the other hand, the
270 average size of the BALF-derived exosomes was ~89.85 nm (avg. conc. = $2.95 \pm 2.2 \times$
271 10^{10} particles/mL) (Figs 1i & 2i). TEM analysis confirmed the morphology of isolated
272 exosomes from BALF and lung tissue samples as shown in Figs 1ii & 2ii.

273 Finally, we used immunoblotting to study the presence of exosome surface markers
274 (CD9, CD81 and CD63) in the isolated exosome fractions from BALF and lung tissues.
275 We found enrichment of positive surface markers for BALF exosomes, such as CD9
276 and CD81 in the isolated exosome fractions (Fig 1iii, full blots in Suppl. Fig 1). Similarly,
277 we found abundance of positive surface markers for tissue exosomes- CD63 and CD81-
278 in the exosome fractions from the lung tissues (Fig 2iii, full blots in Suppl. Fig 2).
279 Overall, our results confirm the successful isolation of exosomes from human BALF and
280 lung tissues in our study groups.

281 **Batch variations in the exosome-derived miRNA expression profiles amongst the** 282 **various study groups**

283 We performed Principal Component analyses (PCA) to visualize the batch variations
284 within the samples. Separate analyses were run for the BALF- and lung tissue-derived
285 exosomes. The plot was generated by using 50 miRNAs with the highest component of
286 variation among groups. Each sample group was clustered using a confidence ellipse
287 as shown in the Fig 3. The PCA plot from lung-derived exosomal miRNAs showed a
288 distinct clustering of the IPF patient samples as compared to the other three study

289 groups, thus suggesting a unique transcriptomic identity of these lung-derived
290 exosomes.

291 **Pairwise comparison of BALF- and lung tissue-derived exosomal miRNAs** 292 **expression profiles**

293 Next, we generated volcano plots showing pairwise comparisons of the differential
294 miRNA expression profiles between various experimental groups in BALF or lung
295 tissue-derived exosomes (Figs 4&5). We plotted the $-\log_{10}$ of adjusted p -values on the
296 Y-axis, and the \log_2 fold change between two experimental groups on the X-axis to
297 generate a volcano plot. Fold changes greater than ± 1 on the logarithmic (base2) scale
298 of thus derived volcano plots were considered significant. miRNAs showing no
299 significant fold change were denoted with blue, while significantly up- or down-regulated
300 miRNAs were denoted with green and red colored dots respectively.

301 **Hierarchical clustering identified differentially expressed miRNAs in the BALF or** 302 **lung-derived exosomes from non-smokers, smokers, patients of COPD and IPF**

303 We generated heat maps showing the top 50 differentially expressed miRNAs from the
304 BALF and lung tissue-derived exosomes from NS vs Sm, NS vs COPD, NS vs IPF and
305 Sm vs COPD as shown in Figs 6 &7 . Each miRNA is depicted in the individual row of
306 the heat map while the color scale represents the relative expression level as denoted
307 in the scale bar alongside. A detailed information about the significantly altered miRNAs
308 with their respective p -values and biological significance has been listed in
309 Supplementary Tables 1&2. In brief, the following observations were made on
310 comparing the various experimental pairs:

311 **Non-smokers vs Smokers:** We did not detect any significant differentially expressed
312 miRNA in the BALF-derived exosomes from smokers and non-smokers. Similarly, no
313 significant variation was observed on comparing the miRNA population from lung tissue-
314 derived exosomes from smokers and non-smokers.

315 **Non-smokers vs COPD:** On comparing the BALF derived exosomal miRNAs from non-
316 smokers and COPD patients, we found three significant differentially expressed
317 miRNAs. Of these, two (miR-320b and miR-22-3p) were significantly upregulated, while
318 one (miR-423-5p) was significantly downregulated in the BALF-derived exosomes from
319 COPD patients as compared to the non-smoking controls. In contrast, we demonstrated
320 significant downregulation of one (miR-122-5p) exosomal miRNA in the lung-tissues of
321 COPD patients as compared to non-smokers.

322 **Smoker vs COPD:** We observed significant downregulation of miR-100-5p in the BALF-
323 derived exosomes from COPD patients in comparison to those from healthy smokers.

324 Similarly, on comparing the lung-derived exosomes from these two study groups we
325 found a significant downregulation of one miRNA. We noticed a significant
326 downregulation of miR-122-5p in the exosomes derived from the lungs of COPD
327 patients as compared to healthy smokers. Interestingly, the same miRNA was found to
328 be downregulated on comparing the miRNA population from the lung-derived exosomes
329 from COPD patients and non-smokers.

330 **Non-smokers vs IPF:** Our results showed a distinct miRNA signature in the BALF and
331 lung tissue-derived exosomes from IPF patients as compared to non-smoking controls.
332 A total of nine differentially expressed miRNAs were identified from the BALF-derived

333 exosomes of IPF patients as compared to healthy non-smoking controls. Of the 9, five
334 (miR-375-3p, miR-200a-3p, miR-200b-3p, miR-141-3p, and miR-423-5p) miRNAs were
335 significantly downregulated; while four (miR-22-3p, miR-320a-3p, miR-320b, and miR-
336 24-3p) were upregulated in the BALF of IPF patients.

337 Interestingly, we found 55 (26 upregulated and 29 downregulated) differentially
338 expressed miRNAs in the lung-derived exosomes from lungs of IPF patients as
339 compared to non-smoking controls.

340 **GO enrichment and KEGG analyses differentially expressed miRNAs from BALF** 341 **and lung-derived exosomes in COPD and IPF patients**

342 To understand the potential functions of the differentially expressed miRNAs in COPD
343 and IPF patients, we performed GO enrichment covering three major domains-
344 biological process, cellular compartment and molecular function. GO term annotation of
345 differentially altered miRNAs in BALF-derived exosomes from COPD patients as
346 compared to healthy non-smokers and smokers resulted in enrichment of terms
347 including: post-translational protein modification, ubiquinone biosynthetic process,
348 cellular component organization, membrane enclosed lumen, clathrin-coated vesicle,
349 mitochondrial matrix, protein binding, protein heterodimerization and transferase
350 activity. The regulatory pathway annotation by KEGG enrichment analyses showed
351 representation of pathways involved in terpenoid backbone biosynthesis, cAMP
352 signaling, cellular senescence and chemokine signaling amongst COPD patients.
353 However, none of these pathways was significantly over-represented in our analyses.
354 GO annotation for miRNA population obtained from IPF patient BALF resulted in
355 enrichment of terms including, lipid transport, mesenchymal cell development,

356 chromatin, mitochondria, lysosome, R-SMAD binding and ATPase activity. The KEGG
357 analyses for this subject group showed 80% overlap with the pathways enriched
358 amongst COPD patients. Interestingly, however, we found a significant
359 overrepresentation of pathways regulating glycosaminoglycan biosynthesis ($p=0.028$) in
360 the BALF-derived exosomes from IPF patients.

361 GO annotation of differentially regulated miRNAs from lung derived exosomes was
362 conducted separately. We found enrichment of terms like, blood vessel morphogenesis,
363 angiogenesis, transmembrane signaling receptor activity, G protein-coupled receptor
364 activity, calcium mediated signaling and calcineurin-NFAT signaling cascade in lung-
365 derived exosomes from COPD patients as compared to healthy individuals (non-
366 smokers and smokers). Contrarily, GO terms including, plasma membrane bounded cell
367 projection organization, chemical homeostasis, G protein-coupled receptor activity,
368 positive regulation of phospholipase C activity, MHC class II protein complex signaling,
369 GTPase activator activity, and positive regulation of non-membrane spanning protein
370 tyrosine kinase activity were found to be enriched on analyzing differentially expressed
371 miRNAs from lung-derived exosomes in IPF patients. KEGG enrichment analyses
372 showed overrepresentation of pathways regulating apoptosis, asthma, and cGMP-PKG
373 signaling pathway, amongst others in COPD patients. However, none of these
374 regulatory pathways were significantly represented. Contrarily, KEGG enrichment
375 analyses of miRNA profile from IPF patients identified representation of 40 pathways, of
376 which 12 were significantly represented in the miRNA population from the lung-derived
377 exosomes from IPF patients.

378 Tables 2-5 provide an account of the GO enrichment and KEGG analyses results for
379 our comparisons of various subject groups in this study. Only selected pathways has
380 been represented in the Tables.

381

382 **Discussion**

383 The role of exosomes in lung diseases has gained increasing attention in recent times
384 due to their role in influencing intercellular communication. These are 50-150 nm in
385 diameter, membrane-bound vesicles that contain protein, DNA, mRNA, microRNA
386 (miRNA) and small non-coding RNAs to regulate pleiotropic functions(41). Recent
387 studies suggest that exosomes mediate cellular crosstalk in lung microenvironment and
388 that cigarette smoke-induced exosomes promote myofibroblast differentiation in primary
389 lung fibroblasts (21, 22). In addition, activated exosomes (due to cigarette smoke or
390 disease conditions) result in macrophage polarization and matrix destruction in mouse
391 models (42, 43). These studies implicate that exosomes affect cell-to-cell signaling in
392 tobacco smoke-related disorders.

393 In this respect, inhalation of toxic agents from tobacco smoke might result in irreparable
394 airway injury leading to various lung diseases like COPD and IPF. While the
395 etiology/cause of each of these diseases might be environmental factors, the disease
396 pathologies are distinct (41). Therefore, we were interested in understanding if the
397 exosomal population and the exosome-derived miRNA signatures from BALF and lung
398 tissues of non-smokers, smokers, COPD patients and IPF patients are unique and can

399 be developed into effective biomarkers for the clinical diagnosis of respective
400 pathologies.

401 Results from next generation sequencing revealed no significant differentially expressed
402 miRNAs in the BALF or lung-derived exosomes from healthy smokers and non-smokers.
403 This suggests that smoking status alone does not affect the exosome-mediated
404 signaling in healthy individuals. However, we found a distinct variation in the miRNA
405 populations from BALF and lung tissue-derived exosomes from COPD patients in
406 comparison to healthy non-smokers. We found a 3-fold downregulation in the
407 expression of miR-423-5p in the BALF-derived exosomes from COPD patients as
408 compared to healthy non-smoking controls. Of note, miR-423-5p is known to be
409 involved in the regulation of apoptosis and extracellular matrix degradation in human
410 nucleus pulposus cells (44). Contrary to our findings, Molina-Pinelo *et al* (2014)
411 identified increased expression of miR-423-5p in the BALF collected from COPD
412 patients as compared to the control group. However, it is important to mention here that
413 the control group included in this study comprised of a few ex- smokers and they did not
414 look at the exosome-derived miRNA from BALF (45). So taken together, it can be
415 concluded that miR-423-5p is crucial in COPD and must be studied further to
416 understand its potential role in the pathophysiology of COPD.

417 Further, we observed two-fold increase in the expression of miR-320b and miR-22-3p in
418 the BALF-derived exosomes from COPD patients as compared to the non-smoking
419 controls. Previous study by our group identified upregulation of both miR-320b and miR-
420 22-3p in the peripheral blood-derived exosomes of COPD patients (11), thus indicating
421 significant role of these miRNAs in regulating the disease phenotype. miR-320b is the

422 negative regulator of mitochondrial mediator, TP53-regulated inhibitor of apoptosis
423 (TRIAP1), and has been previously shown to be upregulated in the peripheral blood
424 nuclear cells (PBMCs) from COPD patients (46, 47). Similarly, miR-22-3p is reported to
425 inhibit HDAC4 to promote Th17-mediated emphysema in cigarette smoke (4 month)-
426 exposed C57Bl/6 mice lungs (48). Serum levels of miR-22-3p are known to be
427 increased amongst COPD patients based on their history of smoking, thus revealing the
428 crucial nature of this miRNA in the progression of the disease (49).

429 On comparing the miRNA expression of lung tissue-derived exosomes from COPD
430 patients and non-smokers, we observed 3-fold downregulation of miR-122-5p in the
431 lungs of COPD patients as compared to healthy non-smoking controls. Importantly, we
432 further observed a 5-fold decrease in the expression of miR-122-5p on comparing
433 miRNA population from lung-derived exosomes from COPD patients versus healthy
434 smokers. Our results are in accordance with previous literature (50-52). For instance,
435 Zhu *et al* (2020) demonstrated the downregulation of miR-122-5p in the sputum and
436 plasma of COPD patients and proved that it functions as a negative regulator of IL-17A
437 production (50). It is pertinent to mention here that though we did not find any commonly
438 altered miRNAs in the exosomes from BALF or lung tissues of COPD patients, we
439 found links that associate miRNA-mediated modulation of IL17-signalling amongst the
440 diseased individual. The role of IL-17 in the disease pathology of COPD is rapidly
441 emerging and is known to play an important role in the regulation of chronic
442 inflammation and emphysema in COPD (53). Hence, our findings identify the upstream
443 regulators of this pathway that could possibly alter the IL17-mediated inflammation in
444 patients with advancing disease.

445 Next, we identified significant downregulation of miR-100-5p in the BALF-derived
446 exosomes from COPD patients as compared to healthy smokers. Functionally, miR-100
447 has been linked to the regulation of epithelial-mesenchymal transition (EMT), apoptosis
448 and inflammation (54, 55). Furthermore, Akbas and colleagues have demonstrated
449 downregulation of miR-100-5p in the serum of COPD patients when compared to
450 healthy smokers, which is in accordance to our study results (56).

451 The differentially expressed miRNA population from BALF and lung tissue-derived
452 exosomes in COPD and IPF was very distinct in our study. We found five significantly
453 downregulated (miR-200a-3p, miR-200b-3p, miR-141-3p, miR-375-3p, and miR-423-3p)
454 whereas four significantly upregulated (miR-320a-3p, miR-320b, miR-22-3p and miR-
455 24-3p) miRNAs in the BALF-derived exosomes from IPF patients. Of these, miR-423-3p
456 and miR-320b were found to be significantly dysregulated amongst COPD patients as
457 well. Of note, existing reports suggest a role of miR-200 in the pathogenesis of IPF (57,
458 58). It has been shown that miR-200 promotes TGF- β 1-induced EMT in normal cells
459 and its downregulation results in fibrogenic phenotype in IPF (57). To our knowledge,
460 there is no existing literature associating miR-141-3p, miR-22-3p and miR-24-3p with
461 IPF. Thus, we for the first time identify the association of these miRs with the disease
462 pathogenesis in IPF.

463 We found 55 differentially expressed miRNAs in the lung-derived exosomes from IPF
464 patients when compared to non-smokers. Of these, many including miR514-3p, miR-
465 122-5p, miR-10b-5p, miR-139b-3p, miR-582-5p, miR-889-3p, miR-1-3p, miR-148a-3p
466 and miR-151b, have never been reported with IPF. Our study for the first time reports
467 the correlation of the dysregulated expression of these miRNAs in the lung derived

468 exosomes from IPF patients. Of note, we observed a three-fold increase in the
469 expression of miR-506-3p in the lung-derived exosomes from IPF patients as compared
470 to the healthy non-smoking controls. Previous work by Zhu et al (2019) reported that
471 miR-506-3p targets p65 subunit of NF- κ B to induce apoptosis and inflammation in
472 experimental mice model for IPF. This study concluded that miR-506-3p is a regulator of
473 lung fibrosis (59). Our results provide clinical evidence suggesting a crucial role of this
474 miRNA in the pathophysiology of IPF in humans. Similarly, accumulating evidence
475 support the role of miR-21-5p in the disease progression of IPF (60-62). Further, the
476 expression of miR-21-5p is controlled by the levels of TGF- β family proteins and
477 SMADs, both of which are key regulators in the etiology of fibrosis (63).

478 Our study had some limitations. Firstly, the sample size for each of the study groups
479 was quite small (n=8-16). In addition, due to non-availability of age- and gender-
480 matched individuals in our cohorts, we were unable to normalize for the gender and
481 age-specific bias in our results. Further limitations were the non-availability of non-
482 smokers/never-smokers and limited information regarding the spirometry, pack-years
483 and smoking history of all the subjects included in this study, which may have affected
484 the final interpretation of our findings.

485 **Conclusions**

486 Overall, this is the first study that compares the BALF and lung tissue-derived exosomal
487 miRNAs from IPF and COPD patients with healthy subjects to suggest the unique
488 miRNA signatures that could develop as a biomarker to identify the disease progression
489 of these pulmonary conditions. Future studies will be designed to validate the findings

490 from this work and to understand the role of exosomal miRNAs in affecting the disease
491 development, progression and severity in COPD and IPF.

492 **List of Abbreviations:**

493 COPD: Chronic Obstructive Pulmonary disease

494 IPF: Idiopathic Pulmonary disease

495 TEM: Transmission Electron Microscopy

496 NGS: Next Generation sequencing

497 miRNA: micro RNA

498 BALF: Bronchoalveolar Lavage fluid

499 EMT: epithelial-mesenchymal transition

500

501 **Acknowledgements:** The authors would like to acknowledge Drs. Isaac Sundar
502 and Dongmei Li for their scientific inputs. We would further like to thank Sarah
503 McNamara, research nurse at Centre for Inflammation Research, University of
504 Edinburgh for providing patient care during sample collection for this study. We would
505 like to acknowledge Dr. Robert Foronjy, Associate Professor at SUNY Downstate
506 Health Sciences University for for clinical support for some of the BALF samples
507 included in the study. We would also like to acknowledge Dr. Ashokkumar Srinivasan
508 for his assistance in optimization of study protocol.

509 **Declarations:** The authors have declared that no competing interests exist.

510 **Funding:** The National Institutes of Health (NIH) HL137738, HL133404 and
511 HL135613 supported this work.

512 **Role of the Funder/Sponsor:** The content is solely the responsibility of the authors and
513 does not necessarily represent the official views of the NIH.

514 **Disclaimer:** None

515 **Meeting Presentation:** None

516 **Additional Contributions:** None

517 **Competing interests:** The authors have no competing interests.

518 **Data Availability:** All the data included in this manuscript is available online and is free
519 to access to all readers. The NGS data and/or analyzed files during the current study
520 are available at Gene Expression Omnibus accession number GSE180651
521 (<https://www.ncbi.nlm.nih.gov/geo/query/acc.cgi?acc=GSE180651>). Data available date:
522 August 15-2021.

523 **Availability of data and materials:** All authors confirm the availability of data and
524 materials online/free access to readers.

525 **Authors Contribution:** GK and KPM designed and conducted the experiments, GK
526 and IR wrote, edited and/or revised the manuscript. GK was responsible for data
527 curation, IR conceptually designed the overall experiments and manuscript, and
528 acquired funding. MC, HSC, FL, NK, MAH provided BALF and/or lung tissues and
529 edited the manuscript.

530 **References**

- 531 1. Sousa C, Rodrigues M, Carvalho A, Viamonte B, Cunha R, Guimarães S, et al. Diffuse smoking-
532 related lung diseases: insights from a radiologic-pathologic correlation. *Insights Imaging*. 2019;10(1):73-
533 2. Ryu JH, Colby TV, Hartman TE, Vassallo R. Smoking-related interstitial lung diseases: a concise
534 review. *European Respiratory Journal*. 2001;17(1):122.

- 535 3. Chilosi M, Poletti V, Rossi A. The pathogenesis of COPD and IPF: distinct horns of the same devil?
536 *Respir Res.* 2012;13(1):3-.
- 537 4. Devine JF. Chronic obstructive pulmonary disease: an overview. *Am Health Drug Benefits.*
538 2008;1(7):34-42.
- 539 5. Glassberg MK. Overview of idiopathic pulmonary fibrosis, evidence-based guidelines, and recent
540 developments in the treatment landscape. *The American journal of managed care.* 2019;25(11
541 Suppl):S195-s203.
- 542 6. O'Farrell HE, Yang IA. Extracellular vesicles in chronic obstructive pulmonary disease (COPD). *J*
543 *Thorac Dis.* 2019;11(Suppl 17):S2141-S54.
- 544 7. Wang N, Wang Q, Du T, Gabriel ANA, Wang X, Sun L, et al. The Potential Roles of Exosomes in
545 Chronic Obstructive Pulmonary Disease. *Front Med (Lausanne).* 2021;7:618506-.
- 546 8. Minnis P, Kane R, Anglin R, Walsh S, Worrel J, Khan F, et al. Serum exosomes from IPF patients
547 display a fibrotic miRNA profile that correlates to clinical measures of disease severity. *European*
548 *Respiratory Journal.* 2015;46(suppl 59):PA3845.
- 549 9. Njock M-S, Guiot J, Henket MA, Nivelles O, Thiry M, Dequiedt F, et al. Sputum exosomes:
550 promising biomarkers for idiopathic pulmonary fibrosis. *Thorax.* 2019;74(3):309.
- 551 10. Mohan A, Agarwal S, Clauss M, Britt NS, Dhillon NK. Extracellular vesicles: novel communicators
552 in lung diseases. *Respir Res.* 2020;21(1):175.
- 553 11. Sundar IK, Li D, Rahman I. Small RNA-sequence analysis of plasma-derived extracellular vesicle
554 miRNAs in smokers and patients with chronic obstructive pulmonary disease as circulating biomarkers.
555 *Journal of extracellular vesicles.* 2019;8(1):1684816.
- 556 12. Sundar IK, Li D, Rahman I. Proteomic Analysis of Plasma-Derived Extracellular Vesicles in
557 Smokers and Patients with Chronic Obstructive Pulmonary Disease. *ACS Omega.* 2019;4(6):10649-61.
- 558 13. Sundar IK, Yao H, Rahman I. Oxidative stress and chromatin remodeling in chronic obstructive
559 pulmonary disease and smoking-related diseases. *Antioxidants & redox signaling.* 2013;18(15):1956-71.
- 560 14. Lerner CA, Sundar IK, Rahman I. Mitochondrial redox system, dynamics, and dysfunction in lung
561 inflammaging and COPD. *The international journal of biochemistry & cell biology.* 2016;81(Pt B):294-
562 306.
- 563 15. Takahashi T, Kobayashi S, Fujino N, Suzuki T, Ota C, He M, et al. Increased circulating endothelial
564 microparticles in COPD patients: a potential biomarker for COPD exacerbation susceptibility. *Thorax.*
565 2012;67(12):1067-74.
- 566 16. Lacedonia D, Carpagnano GE, Trotta T, Palladino GP, Panaro MA, Zoppo LD, et al. Microparticles
567 in sputum of COPD patients: a potential biomarker of the disease? *International journal of chronic*
568 *obstructive pulmonary disease.* 2016;11:527-33.
- 569 17. Tan DBA, Armitage J, Teo TH, Ong NE, Shin H, Moodley YP. Elevated levels of circulating
570 exosome in COPD patients are associated with systemic inflammation. *Respiratory medicine.*
571 2017;132:261-4.
- 572 18. Eltom S, Dale N, Raemdonck KR, Stevenson CS, Snelgrove RJ, Sacitharan PK, et al. Respiratory
573 infections cause the release of extracellular vesicles: implications in exacerbation of asthma/COPD. *PLoS*
574 *one.* 2014;9(6):e101087.
- 575 19. Gordon C, Gudi K, Krause A, Sackrowitz R, Harvey BG, Strulovici-Barel Y, et al. Circulating
576 endothelial microparticles as a measure of early lung destruction in cigarette smokers. *American journal*
577 *of respiratory and critical care medicine.* 2011;184(2):224-32.
- 578 20. Shen Y, Wang L, Wu Y, Ou Y, Lu H, Yao X. A novel diagnostic signature based on three circulating
579 exosomal miRNAs for chronic obstructive pulmonary disease. *Exp Ther Med.* 2021;22(1):717-.
- 580 21. Fujita Y, Araya J, Ito S, Kobayashi K, Kosaka N, Yoshioka Y, et al. Suppression of autophagy by
581 extracellular vesicles promotes myofibroblast differentiation in COPD pathogenesis. *J Extracell Vesicles.*
582 2015;4:28388-.

- 583 22. Bartel S, Deshane J, Wilkinson T, Gabrielsson S. Extracellular Vesicles as Mediators of Cellular
584 Cross Talk in the Lung Microenvironment. *Front Med (Lausanne)*. 2020;7:326-.
- 585 23. Salimian J, Mirzaei H, Moridikia A, Harchegani AB, Sahebkar A, Salehi H. Chronic obstructive
586 pulmonary disease: MicroRNAs and exosomes as new diagnostic and therapeutic biomarkers. *Journal of*
587 *research in medical sciences : the official journal of Isfahan University of Medical Sciences*. 2018;23:27.
- 588 24. Savarimuthu Francis SM, Davidson MR, Tan ME, Wright CM, Clarke BE, Duhig EE, et al.
589 MicroRNA-34c is associated with emphysema severity and modulates SERPINE1 expression. *BMC*
590 *genomics*. 2014;15:88.
- 591 25. Guiot J, Njock M-S, Henket M, Nivelles O, Louis R, Struman I. Sputum exosomal microRNAs in
592 IPF. *European Respiratory Journal*. 2018;52(suppl 62):OA2119.
- 593 26. Liu B, Li R, Zhang J, Meng C, Zhang J, Song X, et al. MicroRNA-708-3p as a potential therapeutic
594 target via the ADAM17-GATA/STAT3 axis in idiopathic pulmonary fibrosis. *Experimental & Molecular*
595 *Medicine*. 2018;50(3):e465-e.
- 596 27. Chen YW, Leung JM, Sin DD. A Systematic Review of Diagnostic Biomarkers of COPD
597 Exacerbation. *PloS one*. 2016;11(7):e0158843.
- 598 28. Shaw JG, Vaughan A, Dent AG, O'Hare PE, Goh F, Bowman RV, et al. Biomarkers of progression
599 of chronic obstructive pulmonary disease (COPD). *J Thorac Dis*. 2014;6(11):1532-47.
- 600 29. Roth MD, Connett JE, D'Armiento JM, Foronjy RF, Friedman PJ, Goldin JG, et al. Feasibility of
601 retinoids for the treatment of emphysema study. *Chest*. 2006;130(5):1334-45.
- 602 30. Agudelo CW, Kumley BK, Area-Gomez E, Xu Y, Dabo AJ, Geraghty P, et al. Decreased surfactant
603 lipids correlate with lung function in chronic obstructive pulmonary disease (COPD). *PloS one*.
604 2020;15(2):e0228279.
- 605 31. Maremanda KP, Sundar IK, Li D, Rahman I. Age-Dependent Assessment of Genes Involved in
606 Cellular Senescence, Telomere, and Mitochondrial Pathways in Human Lung Tissue of Smokers, COPD,
607 and IPF: Associations With SARS-CoV-2 COVID-19 ACE2-TMPRSS2-Furin-DPP4 Axis. 2020;11(1356).
- 608 32. Sundar IK, Yin Q, Baier BS, Yan L, Mazur W, Li D, et al. DNA methylation profiling in peripheral
609 lung tissues of smokers and patients with COPD. *Clinical epigenetics*. 2017;9:38.
- 610 33. Dooner MS, Stewart C, Deng Y, Papa E, Pereira M, Del Tatto M, et al. Daily rhythms influence the
611 ability of lung-derived extracellular vesicles to modulate bone marrow cell phenotype. *PloS one*.
612 2018;13(11):e0207444.
- 613 34. Singh K, Maremanda K, Li D, Rahman I. Exosomal microRNAs are novel circulating biomarkers in
614 cigarette, waterpipe smokers, E-cigarette users and dual smokers. *BMC Medical Genomics*. 2020.
- 615 35. Ashburner M, Ball CA, Blake JA, Botstein D, Butler H, Cherry JM, et al. Gene Ontology: tool for
616 the unification of biology. *Nature Genetics*. 2000;25(1):25-9.
- 617 36. Kanehisa M, Goto S, Kawashima S, Nakaya A. The KEGG databases at GenomeNet. *Nucleic acids*
618 *research*. 2002;30(1):42-6.
- 619 37. Robinson MD, Oshlack A. A scaling normalization method for differential expression analysis of
620 RNA-seq data. *Genome biology*. 2010;11(3):R25.
- 621 38. Robinson MD, Smyth GK. Moderated statistical tests for assessing differences in tag abundance.
622 *Bioinformatics (Oxford, England)*. 2007;23(21):2881-7.
- 623 39. Robinson MD, McCarthy DJ, Smyth GK. edgeR: a Bioconductor package for differential
624 expression analysis of digital gene expression data. *Bioinformatics (Oxford, England)*. 2010;26(1):139-40.
- 625 40. Benjamini Y, Hochberg Y. Controlling the False Discovery Rate: A Practical and Powerful
626 Approach to Multiple Testing. 1995;57(1):289-300.
- 627 41. Fujita Y, Kosaka N, Araya J, Kuwano K, Ochiya T. Extracellular vesicles in lung microenvironment
628 and pathogenesis. *Trends in Molecular Medicine*. 2015;21(9):533-42.

- 629 42. Wang L, Chen Q, Yu Q, Xiao J, Zhao H. Cigarette smoke extract-treated airway epithelial cells-
630 derived exosomes promote M1 macrophage polarization in chronic obstructive pulmonary disease.
631 *International immunopharmacology*. 2021;96:107700.
- 632 43. Genschmer KR, Russell DW, Lal C, Szul T, Bratcher PE, Noerager BD, et al. Activated PMN
633 Exosomes: Pathogenic Entities Causing Matrix Destruction and Disease in the Lung. *Cell*. 2019;176(1-
634 2):113-26.e15.
- 635 44. Xu H, Ji L, Yu C, Chen Q, Ge Q, Lu Y. MiR-423-5p Regulates Cells Apoptosis and Extracellular
636 Matrix Degradation via Nucleotide-Binding, Leucine-Rich Repeat Containing X1 (NLRX1) in Interleukin 1
637 beta (IL-1 β)-Induced Human Nucleus Pulposus Cells. *Med Sci Monit*. 2020;26:e922497-e.
- 638 45. Molina-Pinelo S, Pastor MD, Suarez R, Romero-Romero B, González De la Peña M, Salinas A, et
639 al. MicroRNA clusters: dysregulation in lung adenocarcinoma and COPD. *European Respiratory Journal*.
640 2014;43(6):1740.
- 641 46. Dang X, Qu X, Wang W, Liao C, Li Y, Zhang X, et al. Bioinformatic analysis of microRNA and mRNA
642 Regulation in peripheral blood mononuclear cells of patients with chronic obstructive pulmonary
643 disease. *Respir Res*. 2017;18(1):4-.
- 644 47. Li Y, Tang X, He Q, Yang X, Ren X, Wen X, et al. Overexpression of Mitochondria Mediator Gene
645 TRIAP1 by miR-320b Loss Is Associated with Progression in Nasopharyngeal Carcinoma. *PLOS Genetics*.
646 2016;12(7):e1006183.
- 647 48. Lu W, You R, Yuan X, Yang T, Samuel ELG, Marcano DC, et al. The microRNA miR-22 inhibits the
648 histone deacetylase HDAC4 to promote T(H)17 cell-dependent emphysema. *Nat Immunol*.
649 2015;16(11):1185-94.
- 650 49. Velasco-Torres Y, Ruiz V, Montaña M, Pérez-Padilla R, Falfán-Valencia R, Pérez-Ramos J, et al.
651 Participation of the miR-22-HDAC4-DLCO Axis in Patients with COPD by Tobacco and Biomass.
652 *Biomolecules*. 2019;9(12):837.
- 653 50. Zhu K, Zhou S, Xu A, Sun L, Li M, Jiang H, et al. Microbiota Imbalance Contributes to COPD
654 Deterioration by Enhancing IL-17a Production via miR-122 and miR-30a. *Mol Ther Nucleic Acids*.
655 2020;22:520-9.
- 656 51. Osei ET, Florez-Sampedro L, Timens W, Postma DS, Heijink IH, Brandsma C-A. Unravelling the
657 complexity of COPD by microRNAs: it's a small world after all. *European Respiratory Journal*.
658 2015;46(3):807.
- 659 52. Qian Y, Mao Z, Shi Y, Liu Z, Cao Q, Zhang Q. Comprehensive Analysis of miRNA-mRNA-lncRNA
660 Networks in Non-Smoking and Smoking Patients with Chronic Obstructive Pulmonary Disease. *Cellular*
661 *Physiology and Biochemistry*. 2018;50(3):1140-53.
- 662 53. Rich HE, Alcorn JF. IL-17 Strikes a Chord in Chronic Obstructive Pulmonary Disease Exacerbation.
663 *American journal of respiratory cell and molecular biology*. 2018;58(6):669-70.
- 664 54. Liang Y, Zhao G, Tang L, Zhang J, Li T, Liu Z. MiR-100-3p and miR-877-3p regulate overproduction
665 of IL-8 and IL-1 β in mesangial cells activated by secretory IgA from IgA nephropathy patients.
666 *Experimental cell research*. 2016;347(2):312-21.
- 667 55. Han W, Ren X, Yang Y, Li H, Zhao L, Lin Z. microRNA-100 functions as a tumor suppressor in non-
668 small cell lung cancer via regulating epithelial-mesenchymal transition and Wnt/ β -catenin by targeting
669 HOXA1. *Thoracic cancer*. 2020;11(6):1679-88.
- 670 56. Akbas F, Coskunpinar E, Aynaci E, Oltulu YM, Yildiz P. Analysis of serum micro-RNAs as potential
671 biomarker in chronic obstructive pulmonary disease. *Experimental lung research*. 2012;38(6):286-94.
- 672 57. Yang S, Banerjee S, de Freitas A, Sanders YY, Ding Q, Matalon S, et al. Participation of miR-200 in
673 pulmonary fibrosis. *Am J Pathol*. 2012;180(2):484-93.
- 674 58. Moimas S, Salton F, Kosmider B, Ring N, Volpe MC, Bahmed K, et al. miR-200 family members
675 reduce senescence and restore idiopathic pulmonary fibrosis type II alveolar epithelial cell
676 transdifferentiation. *ERJ Open Research*. 2019;5(4):00138-2019.

677 59. Zhu M, An Y, Zhang X, Wang Z, Duan H. Experimental pulmonary fibrosis was suppressed by
678 microRNA-506 through NF-kappa-mediated apoptosis and inflammation. *Cell and Tissue Research*.
679 2019;378(2):255-65.
680 60. Makiguchi T, Yamada M, Yoshioka Y, Sugiura H, Koarai A, Chiba S, et al. Serum extracellular
681 vesicular miR-21-5p is a predictor of the prognosis in idiopathic pulmonary fibrosis. *Respir Res*.
682 2016;17(1):110-.
683 61. Ma X, Kumar M, Choudhury SN, Becker Buscaglia LE, Barker JR, Kanakamedala K, et al. Loss of
684 the miR-21 allele elevates the expression of its target genes and reduces tumorigenesis. *Proceedings of*
685 *the National Academy of Sciences of the United States of America*. 2011;108(25):10144-9.
686 62. Li YF, Jing Y, Hao J, Frankfort NC, Zhou X, Shen B, et al. MicroRNA-21 in the pathogenesis of
687 acute kidney injury. *Protein & cell*. 2013;4(11):813-9.
688 63. Davis BN, Hilyard AC, Lagna G, Hata A. SMAD proteins control DROSHA-mediated microRNA
689 maturation. *Nature*. 2008;454(7200):56-61.
690

691 Tables

692 **Table1: Clinical characteristics of study subjects**

Characteristics	Non-Smokers	Smokers	COPD/Emphysema	IPF	p-value*
BALF					
N	8	8	16	8	
Age (yrs), mean (SD)	49.6 (17.3)	57.4 (8.9)	65.9 (13.3)	76.5 (11.4)	0.0029
Gender					0.2952
Male n (%)	3 (37.5)	2 (25)	7 (38.9)	6 (75)	
N/A	—	—	2	—	
Smoking Status					0.9719
Current Smoker	-	6	2	-	
Ex-smoker	-	2	6	4	
N/A	-	-	7	-	
Lung Tissues					
N	8	8	8	8	
Age (yrs), mean (SD)	48.3 (16.3)	53.8 (15.4)	59.1 (9.9)	68.9 (9.6)	0.0688
Gender					0.981
Male n (%)	4 (50)	6 (75)	3 (37.5)	5 (62.5)	
N/A	2	1	-	-	
Smoking Status					>0.9999

Current Smoker	-	7	2	-	
Ex-smoker	3	1	4	6	
N/A	-	-	1	-	

693 *: Kruskal-Wallis test

694

695 **Table 2: GO Enrichment Analysis of differentially expressed miRNAs in BALF-**
 696 **derived exosomes**

ID	Term	Ontology	n	p-value*
NS vs COPD				
GO:0016043	Cellular component organization	BP	17	0.183535762
GO:0071840	Cellular component organization or biogenesis	BP	17	0.183535762
GO:0061024	membrane organization	BP	3	0.149797571
GO:0051259	protein complex oligomerization	BP	3	0.149797571
GO:0006720	isoprenoid metabolic process	BP	2	0.101214575
GO:0051186	cofactor metabolic process	BP	2	0.101214575
GO:0051188	cofactor biosynthetic process	BP	2	0.101214575
GO:0051262	protein tetramerization	BP	2	0.101214575
GO:0008299	isoprenoid biosynthetic process	BP	2	0.101214575
GO:0006732	coenzyme metabolic process	BP	1	0.051282051
GO:0009108	coenzyme biosynthetic process	BP	1	0.051282051
GO:0006733	oxidoreduction coenzyme metabolic process	BP	1	0.051282051
GO:0043687	post-translational protein modification	BP	1	0.051282051
GO:1901661	quinone metabolic process	BP	1	0.051282051
GO:0042181	ketone biosynthetic process	BP	1	0.051282051
GO:0051290	protein heterotetramerization	BP	1	0.051282051
GO:0051291	protein heterooligomerization	BP	1	0.051282051
GO:0006743	ubiquinone metabolic process	BP	1	0.051282051
GO:0006744	ubiquinone biosynthetic process	BP	1	0.051282051
GO:1901663	quinone biosynthetic process	BP	1	0.051282051
GO:0031974	membrane-enclosed lumen	CC	11	0.007422402
GO:0070013	intracellular organelle lumen	CC	11	0.007422402
GO:0030659	cytoplasmic vesicle membrane	CC	5	0.24291498
GO:0044431	Golgi apparatus part	CC	5	0.24291498
GO:0044429	mitochondrial part	CC	3	0.149797571
GO:1902494	catalytic complex	CC	3	0.149797571
GO:1990234	transferase complex	CC	2	0.101214575
GO:0005788	endoplasmic reticulum lumen	CC	2	0.101214575
GO:0030133	transport vesicle	CC	2	0.101214575
GO:0005802	trans-Golgi network	CC	1	0.051282051
GO:0030135	coated vesicle	CC	1	0.051282051

GO:0030136	clathrin-coated vesicle	CC	1	0.051282051
GO:0030662	coated vesicle membrane	CC	1	0.051282051
GO:0030665	clathrin-coated vesicle membrane	CC	1	0.051282051
GO:0005759	mitochondrial matrix	CC	1	0.051282051
GO:0016765	transferase activity, transferring alkyl or aryl (other than methyl) groups	MF	2	0.101214575
GO:0046982	protein heterodimerization	MF	1	0.051282051
GO:0000010	trans-hexaprenyltranstransferase activity	MF	1	0.051282051
GO:0050347	trans-octaprenyltranstransferase activity	MF	1	0.051282051
Sm Vs COPD				
GO:0007623	circadian rhythm	BP	4	0.114285714
GO:0048511	rhythmic process	BP	4	0.114285714
GO:1901566	organonitrogen compound biosynthetic process	BP	4	0.114285714
GO:1901135	carbohydrate derivative metabolic process	BP	3	0.085714286
GO:1901137	carbohydrate derivative biosynthetic process	BP	2	0.057142857
GO:0006022	aminoglycan metabolic process	BP	1	0.028571429
GO:0006023	aminoglycan biosynthetic process	BP	1	0.028571429
GO:0006024	glycosaminoglycan biosynthetic process	BP	1	0.028571429
GO:0005794	glycosaminoglycan metabolic process	BP	1	0.028571429
GO:0030203	bounding membrane of organelle	CC	8	0.228571429
GO:0001904	organelle subcompartment	CC	6	0.171428571
GO:0044431	Golgi apparatus	CC	6	0.171428571
GO:0098588	Golgi subcompartment	CC	5	0.142857143
GO:0098791	Golgi membrane	CC	4	0.114285714
GO:0016740	transferase activity	MF	5	0.142857143
GO:0016782	transferase activity, transferring sulphur-containing groups	MF	1	0.028571429
GO:0008146	sulphotransferase activity	MF	1	0.028571429
GO:0034483	heparan sulphate sulphotransferase activity	MF	1	0.028571429
GO:0033871	(heparan sulphate)-glucosamine-3-sulphotransferase-2-activity	MF	1	0.028571429
NS vs IPF				
GO:0009636	response to toxic substance	BP	2	0.142682927
GO:0097324	melanocyte migration	BP	1	0.073170732
GO:0097324	melanosome organization	BP	1	0.073170732
GO:0014031	mesenchymal cell development	BP	1	0.073170732
GO:0034204	lipid transport	BP	1	0.073170732
GO:0044429	mitochondrial part	CC	3	0.010787992
GO:0005739	mitochondrion	CC	5	0.034709193
GO:0030136	clathrin-coated vesicle	CC	1	0.073170732
GO:0000785	chromatin	CC	1	0.073170732
GO:0005766	primary lysosome	CC	1	0.073170732

GO:0000010	trans-hexaprenyltranstransferase activity	MF	1	0.073170732
GO:0050347	trans-octaprenyltranstransferase activity	MF	1	0.073170732
GO:0016887	ATPase activity	MF	1	0.073170732
GO:0070412	R-SMAD binding	MF	1	0.073170732

697 *p-value for genes that were significantly up- or downregulated.

698 here BP = biological process; CC= cellular component and MF= molecular function

699 **Table 3: GO Enrichment Analysis of differentially expressed miRNAs in Lung**
 700 **tissue-derived exosomes**

ID	Term	Ontology	n	p-value*
NS vs COPD				
GO:0048514	blood vessel morphogenesis	BP	12	0.068181818
GO:0050808	synapse organization	BP	11	0.0625
GO:0051962	positive regulation of nervous system development	BP	11	0.0625
GO:0044089	positive regulation of cellular component biogenesis	BP	10	0.056818182
GO:0044430	cytoskeletal part	CC	9	0.051136364
GO:0001525	angiogenesis	BP	8	0.045454545
GO:0050803	regulation of synapse structure or activity	BP	8	0.045454545
GO:0050807	regulation of synapse organization	BP	8	0.045454545
GO:0015630	microtubule cytoskeleton	CC	8	0.045454545
GO:0038023	signaling receptor activity	MF	8	0.045454545
GO:0060089	molecular transducer activity	MF	8	0.045454545
GO:0004888	transmembrane signaling receptor activity	MF	7	0.039772727
GO:0004930	G protein-coupled receptor activity	MF	7	0.039772727
GO:0019932	second messenger-mediated signaling	BP	6	0.034090909
GO:0007416	synapse assembly	BP	6	0.034090909
GO:0045765	regulation of angiogenesis	BP	5	0.028409091
GO:1901342	regulation of vasculature development	BP	5	0.028409091
GO:0051963	regulation of synapse assembly	BP	5	0.028409091
GO:0051965	positive regulation of synapse assembly	BP	4	0.022727273
GO:0019722	calcium-mediated signaling	BP	4	0.022727273
GO:0005815	microtubule organizing center	CC	4	0.022727273
GO:0005813	centrosome	CC	4	0.022727273
GO:0016525	negative regulation of angiogenesis	BP	3	0.017045455
GO:1901343	negative regulation of vasculature development	BP	3	0.017045455
GO:2000181	negative regulation of blood vessel morphogenesis	BP	3	0.017045455
GO:0033173	calcineurin-NFAT signaling cascade	BP	2	0.011363636

GO:0048016	inositol phosphate-mediated signaling	BP	2	0.011363636
GO:0097720	calcineurin-mediated signaling	BP	2	0.011363636
<i>Sm Vs COPD</i>				
GO:0048514	blood vessel morphogenesis	BP	11	0.071428571
GO:0044087	regulation of cellular component biogenesis	BP	11	0.071428571
GO:0044089	positive regulation of cellular component biogenesis	BP	10	0.064935065
GO:0051962	positive regulation of nervous system development	BP	10	0.064935065
GO:0001525	angiogenesis	BP	8	0.051948052
GO:0050803	regulation of synapse structure or activity	BP	8	0.051948052
GO:0050807	regulation of synapse organization	BP	8	0.051948052
GO:0044430	cytoskeletal part	CC	7	0.045454545
GO:0038023	signaling receptor activity	MF	7	0.045454545
GO:0060089	molecular transducer activity	MF	7	0.045454545
GO:0019932	second-messenger-mediated signaling	BP	6	0.038961039
GO:0007416	synapse assembly	BP	6	0.038961039
GO:0015630	microtubule cytoskeleton	CC	6	0.038961039
GO:0004888	transmembrane signaling receptor activity	MF	6	0.038961039
GO:0045765	regulation of angiogenesis	BP	5	0.032467532
GO:1901342	regulation of vasculature development	BP	5	0.032467532
GO:0051963	regulation of synapse assembly	BP	5	0.032467532
GO:0051965	positive regulation of synapse assembly	BP	4	0.025974026
GO:0019722	calcium-mediated signaling	BP	4	0.025974026
GO:0016525	negative regulation of angiogenesis	BP	3	0.019480519
GO:1901343	negative regulation of vasculature development	BP	3	0.019480519
GO:2000181	negative regulation of blood vessel morphogenesis	BP	3	0.019480519
GO:0005815	microtubule organizing center	CC	3	0.019480519
GO:0005813	centrosome	CC	3	0.019480519
GO:0004930	G-protein coupled receptor activity	MF	3	0.019480519
GO:0033173	calcineurin-NFAT signaling cascade	BP	2	0.012987013
GO:0048016	inositol phosphate-mediated signaling	BP	2	0.012987013
GO:0097720	calcineurin-mediated signaling	BP	2	0.012987013
<i>NS Vs IPF</i>				
GO:0065008	regulation of biological quality	BP	44	0.0327192
GO:0007399	nervous system development	BP	36	0.006858696
GO:0048878	chemical homeostasis	BP	18	0.003415
GO:0030030	cell projection organization	BP	17	0.012599483
GO:0120036	plasma membrane bounded cell	BP	17	0.01259943

	projection organization			
GO:0044459	plasma membrane region	CC	10	0.028105097
GO:0007416	synapse assembly	BP	7	0.006212841
GO:0030424	axon	CC	7	0.0488352
GO:0150034	distal axon	CC	6	0.0305685
GO:0031349	positive regulation of defense response	BP	5	0.016747
GO:0044306	neuron projection terminus	CC	4	0.007341699
GO:0008092	cytoskeletal protein binding	MF	4	0.0073417
GO:0004930	G-protein coupled receptor activity	MF	4	0.083811139
GO:0051965	positive regulation of synapse assembly	BP	4	0.007341699
GO:0010863	positive regulation of phospholipase C activity	BP	2	0.01653348
GO:0043235	receptor complex	CC	2	0.01653348
GO:0023026	MHC class II protein complex binding	MF	2	0.0165335
GO:0005096	GTPase activator activity	MF	2	0.0165335
GO:1903997	positive regulation of non-membrane spanning protein tyrosine kinase activity	BP	2	0.01653348

701 *p-value for genes that were significantly up- or downregulated.

702 here BP = biological process; CC= cellular component and MF= molecular function

703 **Table 4: KEGG Analyses of differentially expressed miRNAs in BALF-derived**
 704 **exosomes from COPD and IPF patients**

705

KEGG pathway	Selected Pathway
COPD⁻	
path:hsa00900	Terpenoid backbone biosynthesis
path:hsa04920	Adipocytokine signaling pathway
path:hsa00520	Amino sugar and nucleotide sugar metabolism
path:hsa04152	AMPK signaling pathway
path:hsa04371	Apelin signaling pathway
path:hsa04140	Autophagy-animal
path:hsa04136	Autophagy-other
path:hsa01040	Biosynthesis of unsaturated fatty acids
path:hsa04024	cAMP signaling pathway
path:hsa04218	Cellular senescence
path:hsa04062	Chemokine signaling pathway
path:hsa00534 [*]	Glycosaminoglycan biosynthesis
IPF[#]	
path:hsa00900	Terpenoid backbone biosynthesis
path:hsa04920	Adipocytokine signaling pathway
path:hsa00520	Amino sugar and nucleotide sugar metabolism

path:hsa04371	Apelin signaling pathway
path:hsa04140	Autophagy-animal
path:hsa04136	Autophagy-other
path:hsa01040	Biosynthesis of unsaturated fatty acids
path:hsa04218	Cellular senescence
path:hsa04062	Chemokine signaling pathway
path: hsa05206	microRNAs in cancer

706 * significantly enriched pathway; - COPD patients vs healthy controls (non-smokers and
 707 smokers); #IPF patients vs healthy non-smokers

708 **Table 5: KEGG Analyses of differentially expressed miRNAs in lung tissue-**
 709 **derived exosomes from COPD and IPF patients**

710

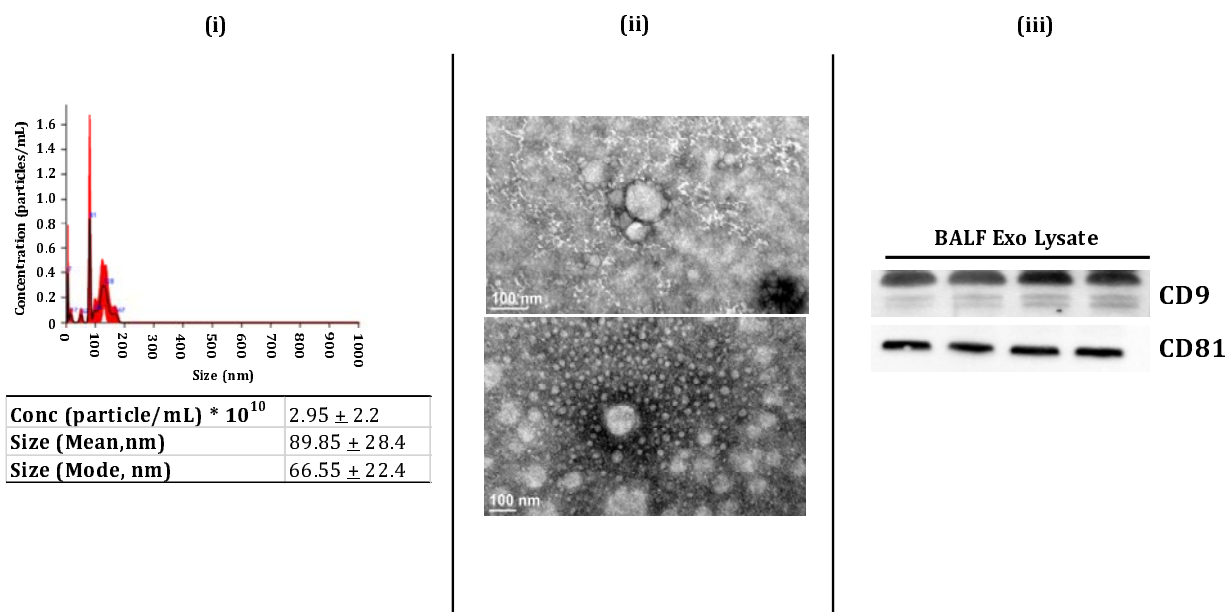
KEGG pathway	Selected Pathway
COPD⁻	
path:hsa04520	Adherens junction
path:hsa04920	Adipocytokine signaling pathway
path:hsa04261	Adrenergic signaling in cardiomyocytes
path:hsa04960	Aldosterone-regulated sodium reabsorption
path:hsa00520	Amino sugar and nucleotide sugar metabolism
path:hsa04215	Apoptosis-multiple species
path:hsa05310	Asthma
path:hsa05100	bacterial invasion of epithelial cells
path:hsa01040	Biosynthesis of unsaturated fatty acids
path:hsa04260	Cardiac muscle contraction
path:hsa04022	cGMP-PKG signaling pathway
IPF[#]	
path:hsa04972 [*]	Pancreatic secretion
path:hsa04970 [*]	Salivary secretion
path:hsa04911 [*]	Insulin secretion
path:hsa05416 [*]	Viral myocarditis
path:hsa05310	Asthma
path:hsa01040	Biosynthesis of unsaturated fatty acids
path:hsa04022	cGMP-PKG signaling pathway

path:hsa04014* Ras signaling pathway
 path:hsa04727* GABAergic synapse
 path:hsa05033* Nicotine addiction
 path:hsa04722* Neurotrophin signaling pathway
 path:hsa04010* MAPK signaling pathway
 path:hsa04151 PI3K-Akt signaling pathway

711 * significantly enriched pathway; - COPD patients vs healthy controls (non-smokers and
 712 smokers); #IPF patients vs healthy non-smokers

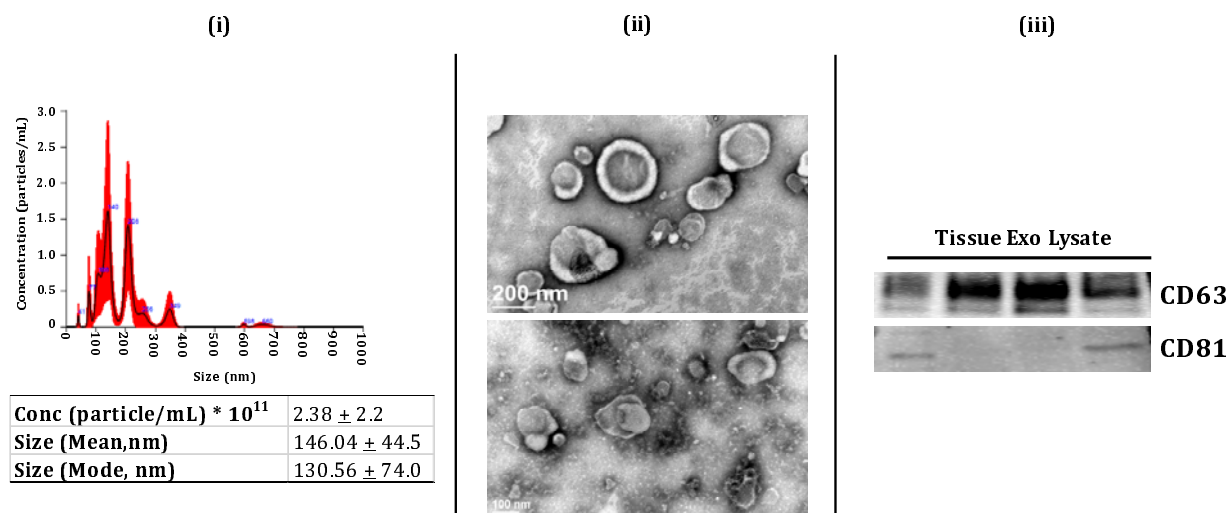
713

714 **Figure and Figure Legends**



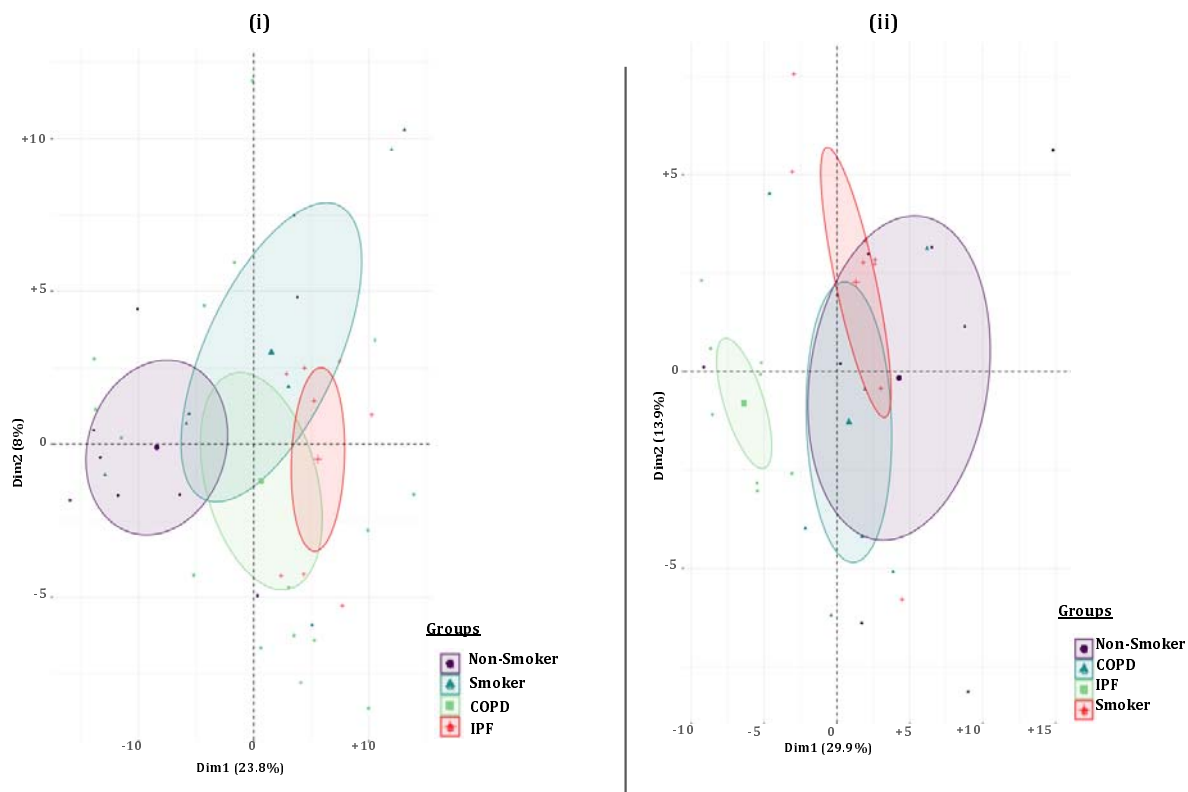
715

716 **Figure 1: Characterization of human BALF-derived EVs/Exosomes.** (i) Particle size
 717 depicted as mean, mode, and particle concentration were estimated using NanoSight
 718 NS300 (n=3-8/group). (ii) Representative TEM images of BALF-derived EVs/Exosomes
 719 (n=3). (iii) Immunoblot analysis of positive (CD9 and CD81) exosomal markers derived
 720 from human BALF (n=4).



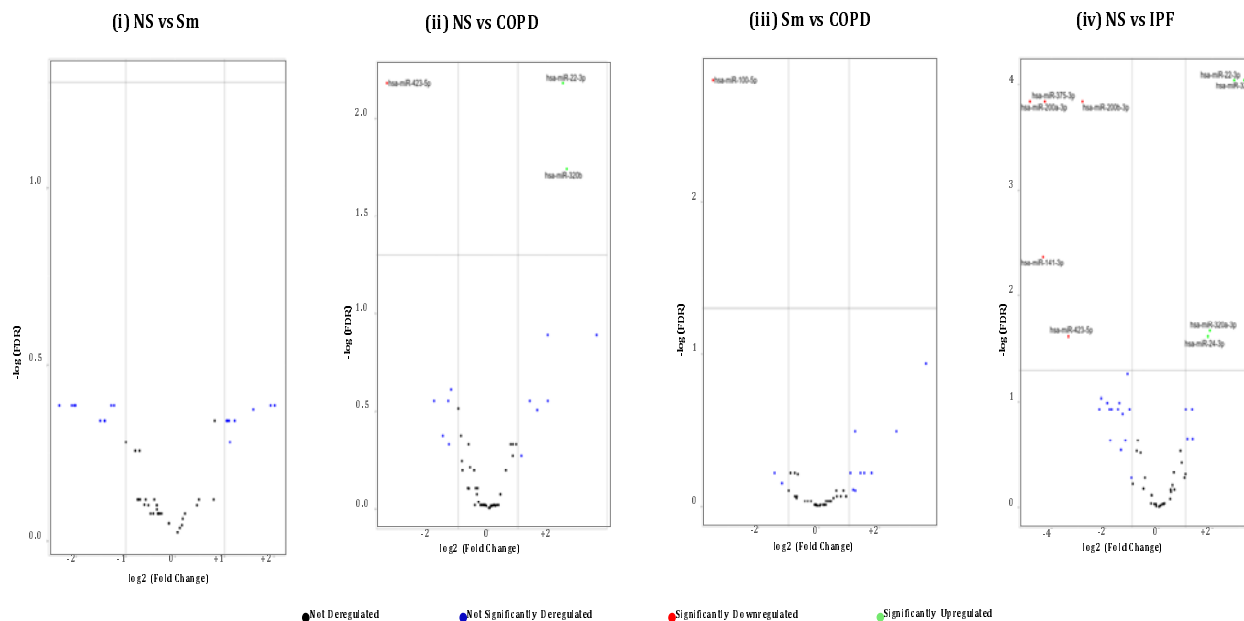
721
722 **Figure 2: Characterization of human lung tissue-derived**
723 **EVs/Exosomes.** (i) Particle size depicted as mean, mode, and particle concentration
724 were estimated using NanoSight NS300 (n=3-5/group). (ii) Representative TEM images
725 of lung tissue-derived EVs/Exosomes (n=6). (iii) Immunoblot analysis of positive (CD63
726 and CD81) exosomal markers derived from human lung tissue (n=4).

727



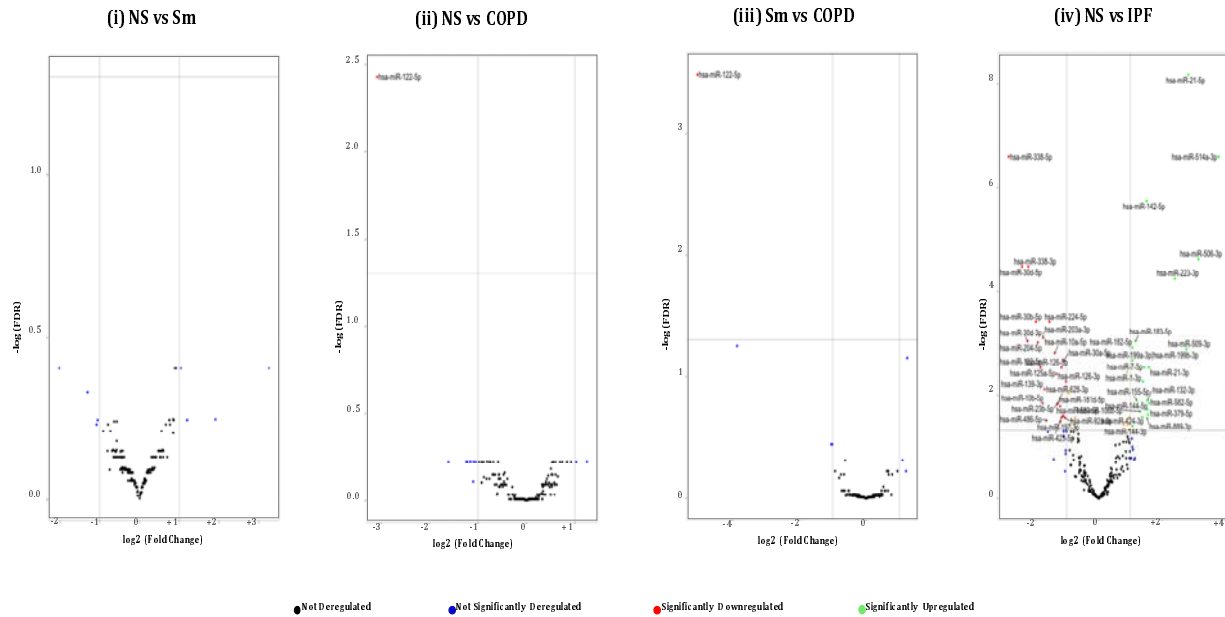
728
729 **Figure 3: Principal Component Plot.** Principal Component Analyses based on
730 differential microRNA expression in individual (i) BALF- and (ii) Lung tissue-derived
731 exosome samples from non-smokers, cigarette smokers, COPD and IPF subjects.

732



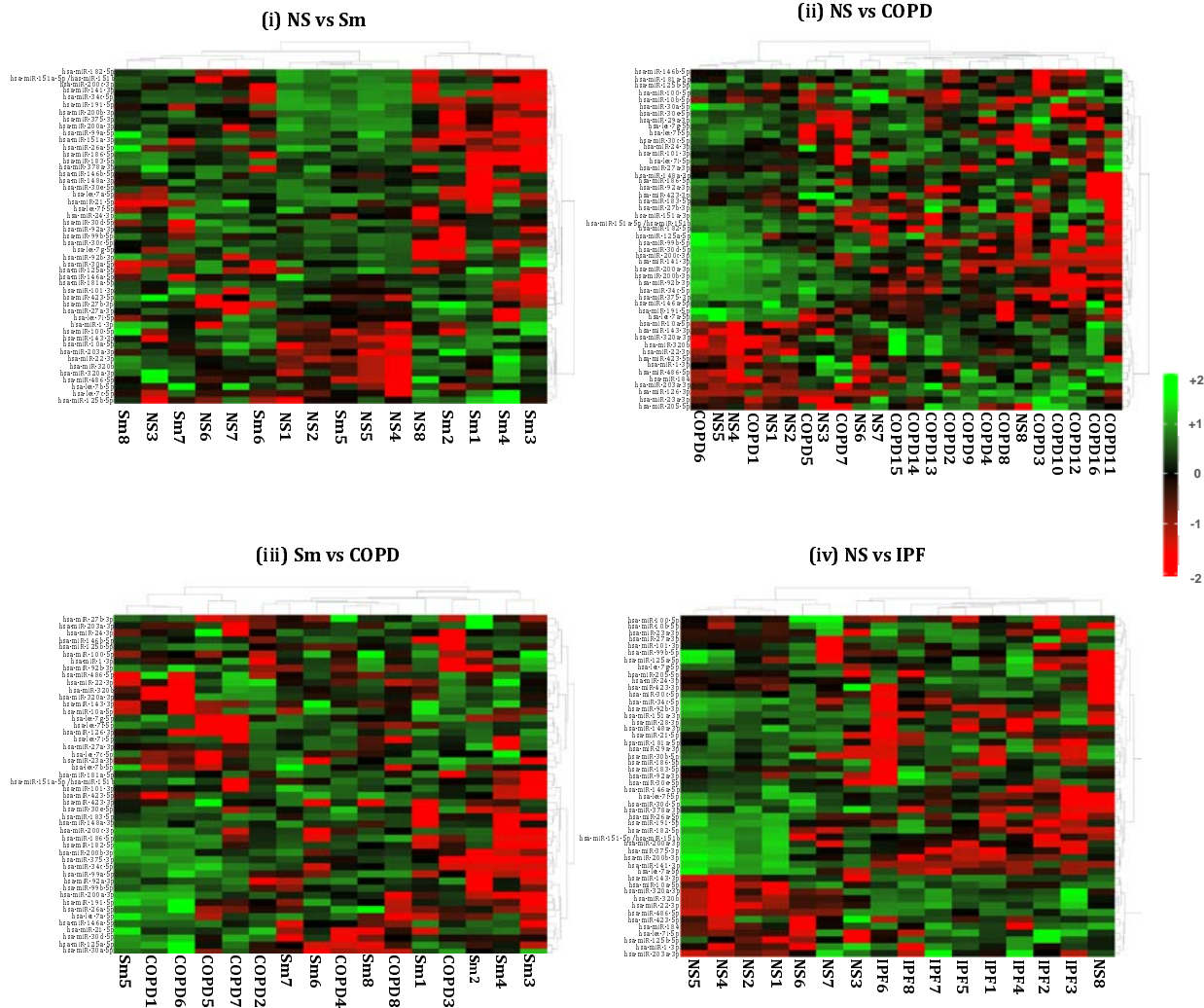
733
734 **Figure 4: Volcano Plots showing number and distribution of miRNA from BALF-**
735 **derived exosomes.** Volcano plot showing the relation between $-\log(\text{FDR})$ [Y-axis] vs
736 $\log_2(\text{fold change})$ [X-axis] in the differentially expressed miRNAs amongst BALF
737 exosomes derived from (i) healthy non-smokers (NS) vs healthy cigarette smokers
738 (Sm), (ii) healthy non-smokers (NS) vs COPD patients (COPD), (iii) healthy cigarette
739 smokers (Sm) vs COPD patients and (iv) healthy non-smokers (NS) and IPF patients
740 (IPF).

741



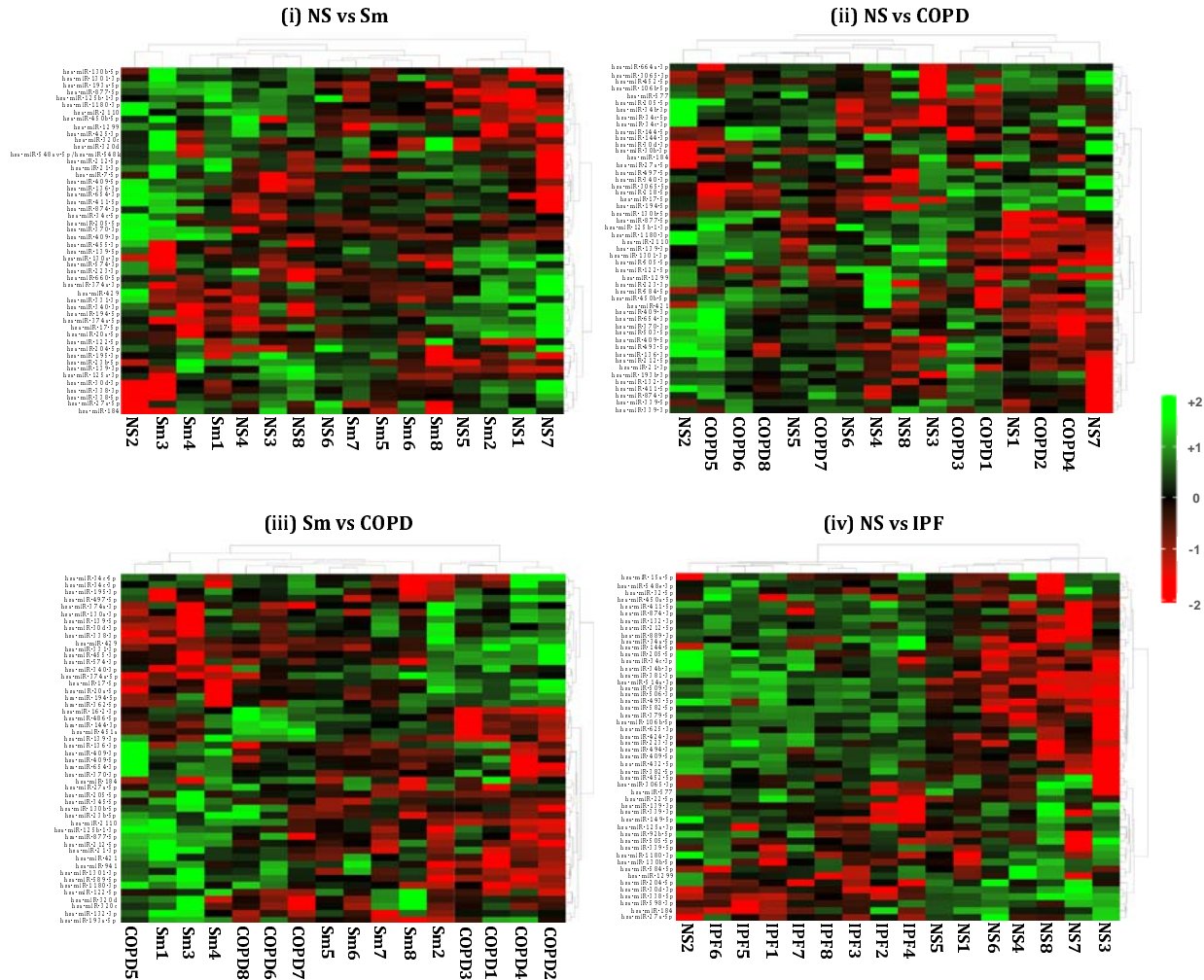
742 **Figure 5: Volcano Plots showing number and distribution of miRNA from lung**
 743 **tissue-derived exosomes.** Volcano plot showing the relation between $-\log(\text{FDR})$ (Y-
 744 axis) vs $\log_2(\text{fold change})$ (X-axis) in the differentially expressed miRNAs amongst lung
 745 tissue exosomes derived from (i) healthy non-smokers (NS) vs healthy cigarette
 746 smokers (Sm), (ii) healthy non-smokers (NS) vs COPD patients (COPD), (iii) healthy
 747 cigarette smokers (Sm) vs COPD patients and (iv) healthy non-smokers (NS) and IPF
 748 patients (IPF).
 749

750



751
 752 **Figure 6: Hierarchical cluster analyses of differentially expressed miRNAs from**
 753 **BALF-derived exosomes.** Heat map showing top 50 variable miRNAs that are
 754 differentially expressed in the BALF-derived exosomes from (i) healthy non-smokers
 755 (NS) vs healthy smokers (Sm), (ii) healthy non-smokers (NS) vs COPD patients
 756 (COPD), (iii) healthy smokers (Sm) and COPD patients (COPD) and (iv) healthy non-
 757 smokers (NS) and IPF patients (IPF).

758



759
 760 **Figure 7: Hierarchical cluster analyses of differentially expressed miRNAs from**
 761 **lung tissue-derived exosomes.** Heat map showing top 50 variable miRNAs that are
 762 differentially expressed in the lung tissue-derived exosomes from (i) healthy non-
 763 smokers (NS) vs healthy smokers (Sm), (ii) healthy non-smokers (NS) vs COPD
 764 patients (COPD), (iii) healthy smokers (Sm) and COPD patients (COPD) and (iv)
 765 healthy non-smokers (NS) and IPF patients (IPF)..

